



Research paper

Hydrodechlorination of trichloroethylene over Pd supported on swellable organically-modified silica (SOMS)



Hyuntae Sohn^a, Gokhan Celik^a, Seval Gunduz^a, Stacey L. Dean^b, Eric Painting^c, Paul L. Edmiston^{b,c,**}, Umit S. Ozkan^{a,*}

^a William G. Lowrie Department of Chemical and Biomolecular Engineering, The Ohio State University, 151 W. Woodruff Avenue, Columbus, OH 43210, USA

^b ABS Materials, Inc., 1909 Old Mansfield Road, Wooster, OH 44691, USA

^c Department of Chemistry, The College of Wooster, 943 College Mall, Wooster, OH 44691, USA

ARTICLE INFO

Article history:

Received 14 July 2016

Received in revised form

12 September 2016

Accepted 11 October 2016

Available online 15 October 2016

Keywords:

SOMS

Organosilica

Hydrodechlorination

Trichloroethylene

Palladium

ABSTRACT

The catalytic activity and resistance to poisoning of Pd catalysts supported on swellable organically-modified silica (SOMS) were investigated for hydrodechlorination (HDC) of trichloroethylene (TCE). The promising catalytic activity of 1% Pd/SOMS sample was attributed to the high affinity of SOMS for organics and its high hydrophobicity. While latter characteristic repels water, the adsorptive capacity for organics allows TCE dissolved in aqueous media to concentrate inside the pores, in the vicinity of the active sites, thus helping the kinetics. In the liquid phase, using a continuous flow reactor, higher TCE conversion was obtained over the 1% Pd/SOMS compared to the commercial 1% Pd/Al₂O₃ catalyst. When the pores of 1% Pd/SOMS sample were fully opened by pre-treating it with ethanol prior to the reaction, HDC activity was seen to significantly increase. In the gas phase, the extent of adsorption was less, reducing the concentration of reactants near the active sites. As a result, 1% Pd/SOMS was less active than 1% Pd/Al₂O₃ for HDC of TCE. To determine their resistance to poisoning, 1% Pd/SOMS and 1% Pd/Al₂O₃ catalysts were poisoned ex-situ with Li₂S. The ex-situ poisoned Pd/SOMS sample maintained its catalytic activity for HDC of TCE. However, a significant loss in catalytic activity of the Pd/Al₂O₃ catalyst was observed after poisoning. Protection from aqueous phase sulfide poisoning was attributed to the hydrophobicity of the Pd/SOMS, which would exclude anionic species from the embedded Pd particles. The XPS, STEM and ICP-OES results indicated that when Pd/Al₂O₃ and Pd/SOMS were treated with 1 M HCl, most of the Pd metal was leached from the Pd/Al₂O₃ catalyst in contrast to Pd/SOMS, which had negligible leaching. Overall, due to hydrophobicity and high affinity for organics, SOMS has potential as a catalyst scaffold for different reactions in groundwater remediation applications.

© 2016 Elsevier B.V. All rights reserved.

1. Introduction

Contamination of groundwater continues to attract public attention due to its importance as a source of drinking water. Trichloroethylene (TCE), which has been extensively used as a metal degreaser [1], is one of the most widely detected volatile organic compound (VOC) contaminants in groundwater [2,3]. The high level of toxicity and the carcinogenic effects of TCE pose a serious threat to the environment and human health [4]. The current groundwater remediation technologies for removal of TCE are

mostly based on adsorption and extraction techniques that require further treatment [5,6]. Therefore, using catalytic processes for TCE remediation, which result in the complete destruction of its chemical structure has many advantages.

Hydrodechlorination (HDC) of TCE is a catalytic reaction where hydrogen is used as a reducing agent to remove chlorine, producing ethane and hydrochloric acid (HCl) as the major products. Among many different precious metals that are used for this process, Pd-based catalysts have exhibited promising catalytic activity for HDC of TCE, especially on alumina or activated carbon (AC) supports [7–12]. Lowry et al. conducted HDC of TCE experiments in liquid phase on 1% Pd/Al₂O₃ and metallic Pd powders. The highest TCE conversion they achieved was 97% for Pd/Al₂O₃, with no by-products observed at room temperature and atmospheric pressure [7]. The Pd particle size was also reported to impact the catalytic activity. Zhang et al. showed that CMC (carboxymethyl

* Corresponding author.

** Corresponding author at: ABS Materials, Inc., 1909 Old Mansfield Road, Wooster, OH 44691, USA.

E-mail addresses: pedmiston@wooster.edu (P.L. Edmiston), ozkan.1@osu.edu (U.S. Ozkan).

cellulose)-stabilized Pd nanoparticles over Al_2O_3 was much more active than the commercial Pd/ Al_2O_3 for liquid phase HDC of TCE [11]. Bimetallic catalysts such as Ni/Fe [13], Pd/Sn [14], Pd/NiMgAl [15], PdCu alloy [16] and Pt and Pd containing Cu-hydrotalcite [17] have also been studied for this reaction. Meshesha et al. have observed close to 100% ethylene selectivity at 300 °C using PdCu alloy nanoparticles supported over Al_2O_3 [16]. The highest TCE hydrodechlorination rate in the literature was reported by Wong and co-workers using bimetallic Pd/Au nanoparticles [18,19]. The authors conducted a comparison study over Pd black powders, Pd/ Al_2O_3 , Pd nanoparticles, Pd/Au nanoparticles, Au/ Al_2O_3 , Au/Pd/ Al_2O_3 and Pd/Au/ Al_2O_3 in terms of their overall catalytic activity. The results exhibited that Pd/Au nanoparticles were significantly more active than other catalysts in aqueous phase for HDC of TCE with a rate constant that was 70 times higher than the commercially available Pd/ Al_2O_3 catalysts on per Pd atom basis. Several additional techniques have been proposed to make the HDC process more economical. One of the more recent methods is the microwave heating that has been presented as an alternative way to heat the reactor up to the desired reaction temperature of TCE HDC [20,21]. In addition, alternative organic hydrogen donors have been explored such as 2-propanol [22] and formic acid [23,24] in liquid phase HDC reactions.

Although Pd-based catalysts have exhibited very good catalytic performance, catalyst deactivation due to ionic poisons dissolved in groundwater is still a recurring issue. For instance, formation of metal-Cl bonds due to chloride ions (Cl^-) in groundwater as well as from the reaction itself has been found to diminish the catalytic performance in hydrodechlorination reactions [17,25–28]. Furthermore, sulfur-containing anions [29] such as sulfate (SO_4^{2-}) and bisulfide (HS^-), and bicarbonate (HCO_3^-) [30] are also poisoning sources which degrade the catalysts.

With respect to chloride poisoning, Ordóñez et al. suggested that the more acidic the support is, the more the affinity it has towards chloride ions [25]. Although the oxidation of metallic Pd under a H_2 environment is not thermodynamically favorable, the presence of chloride ions stabilizes Pd in an oxidized state by forming different complexes, such as PdCl_3^- and PdCl_4^{2-} , thus decreasing the catalyst performance drastically. Their results indicated that Pd/ Al_2O_3 , which is more acidic, showed faster deactivation than Pd/AC for TCE HDC. Moreover, in order to minimize the contact between Pd metal and ionic poisons such as sulfide-containing species, coating materials such as poly-dimethylsiloxane (PDMS) have been tested for HDC reactions [31,32]. This is to enhance the hydrophobicity of the catalysts thereby repelling ionic poisons dissolved in groundwater. However, an associated issue was that HCl produced from the HDC reaction degraded the polymers.

In this study, we attempted to increase the hydrophobicity of the matrix surrounding Pd using a swellable organically-modified silica (SOMS) material as a catalyst scaffold [33–35]. SOMS is extremely hydrophobic and can adsorb a variety of organic molecules including TCE [35]. Another interesting aspect of SOMS is that it consists a crosslinked organosilica network with flexible linkages, thereby allowing a physical volume expansion of the material (swelling). While swelling, it is known to create extra surface area and micropores. The swelling process is reversible through evaporation, in which the volume of the SOMS returns to its original state.

Pd supported on SOMS catalyst has never been investigated for its catalytic activity for HDC of TCE. Therefore, in the present paper, the TCE reaction over the Pd/SOMS catalyst was studied using a continuous flow reactor system both in the liquid and the gas phase. Poisoning and leaching studies were also conducted using Li_2S and HCl, respectively. The catalytic performance of the samples treated with Li_2S and HCl were compared to fresh Pd/SOMS catalysts as well as to commercial Pd/ Al_2O_3 catalyst, which was used as a reference. The HCl-treated Pd/SOMS and Pd/ Al_2O_3 cat-

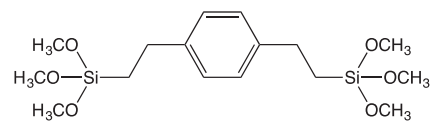


Fig. 1. Bis(trimethoxysilyl)benzene (BTEB).

alysts were characterized by X-ray photoelectron spectroscopy (XPS) and high angle annular dark field (HAADF) scanning transmission electron microscopy (STEM). Inductively coupled plasma optical emission spectrometry (ICP-OES) technique was used measure the extent of Pd leaching of the catalysts. Lastly, the chemical structure, thermal stability, extent of hydrophobicity, surface area and pore volume were examined using RAMAN and infrared (IR) spectroscopy, temperature programmed oxidation (TPO), thermogravimetric analysis (TGA), and N_2 physisorption techniques.

2. Experimental

2.1. Catalyst preparation

The synthesis procedure for SOMS was reported previously by Edmiston and co-workers [33–37]. In brief, it involves a sol-gel synthesis consisting of polycondensation of an aromatically bridged silane precursor (monomer) with flexible linkages between the aryl group and the silicon centers (e.g., [bis(trimethoxysilyl)benzene (BTEB) shown in Fig. 1], followed by hydrolysis and condensation reactions initiated by fluoride ion (e.g., tetrabutyl ammonium fluoride) as a catalyst (leading to Si—O—Si bond formation). Organization of the polycondensed BTEB is aided by p-p stacking interactions of the aryl rings. After aging the gel for 6 days, residual silanol groups are derivatized by end-capping them with organic functional groups (e.g., trimethylchlorosilane ($\text{Si}(\text{CH}_3)_3\text{Cl}$)) which prevents Si—O—Si bond formation during drying, preserving flexibility in the matrix. The crucial step in the synthesis is the choice of the monomer since swelling behavior is observed only when flexible linkages between the aryl group and the silicon centers exist.

1% w/w Pd/SOMS was prepared using Pd(II) acetate (Sigma-Aldrich 98%) through incipient wetness impregnation (IWI) technique. The Pd acetate was first dissolved in acetone and stirred rigorously to obtain a homogenous Pd precursor solution. The mixture was then added to the SOMS support drop-wise using a micropipette at which point the volume of SOMS expanded (swelled). Once the expansion was reached a maximum state, SOMS was dried at 25 °C with constant agitation. The swelling and drying process was repeated until all the precursor solution was added to the SOMS support. Pd^{2+} was reduced by swelling the material with a saturated solution of NaBH_4 in 95% ethanol. The Pd/SOMS particles were then filtered and extensively rinsed with ethanol and then with deionized water, and dried at 60 °C. The particle size of the Pd/SOMS was ~150 μm .

Commercial 1% Pd/ Al_2O_3 was purchased from Sigma-Aldrich. The 1% Pd/ Al_2O_3 was reduced using 5% H_2/He gas at 400 °C for 1 h. The reduction was carried out either ex-situ or in-situ for liquid phase and gas phase reactions, respectively. To desorb any species that may be adsorbed from the atmosphere, the sample was first treated with helium at 450 °C for 30 min.

2.2. Catalyst characterization

2.2.1. Raman and infrared (IR) spectroscopy

Raman spectra were collected with a Renishaw-Smiths Detection Combined Raman-IR Microprobe equipped with Leica and CCD detector (400 × 576). SOMS material was placed on a stainless steel sample holder where a helium-neon laser (633 nm) beam

was focused on a particular spot ($\times 20$ objective). The spectra were collected using an exposure time of 50 s^{-1} in the $300\text{--}4000\text{ cm}^{-1}$ range. FT-IR-ATR spectra were measured using a Thermo Nicolet 6700 FTIR Spectrometer with a diamond attenuated total reflectance accessory.

2.2.2. Temperature programmed oxidation (TPO)

SOMS was placed in a 4 mm-ID quartz reactor, which was then loaded into a Carbolite MTF 10/15/130 furnace. A gas mixture of 5% O_2/He was introduced to the reactor at 30 mL/min at RT and the outlet stream was connected to a mass spectrometer (MKS-Cirrus II) operated in scanning ion mode. The signals from $m/z = 2\text{--}60$ were all monitored in order to detect various products. TPO was performed using a $10\text{ }^\circ\text{C/min}$ temperature ramp rate at which the temperature was increased from RT to $800\text{ }^\circ\text{C}$.

2.2.3. Surface area, pore size and pore volume

Micromeritics ASAP 2020 (accelerated surface area and porosimetry) instrument was used to obtain nitrogen adsorption/desorption isotherms of the SOMS, 1% Pd/SOMS and 1% Pd/ Al_2O_3 catalysts. First, the sample was degassed for 12 h at $130\text{ }^\circ\text{C}$ under $2\text{ }\mu\text{m Hg}$ of vacuum in order to remove any gas molecules captured inside the pores and impurities on the surface. The degassed sample was then transferred to the analysis port where the nitrogen adsorption took place at liquid nitrogen temperature. The collected isotherms were used to calculate the Brunauer-Emmett-Teller (BET) surface area and Brunauer-Joyner-Helena (BJH) pore volumes of the samples. The pore size distribution was obtained from the desorption curve of the isotherm.

2.2.4. High angle annular dark field (HAADF) scanning transmission electron microscopy (STEM) and energy-dispersive X-ray analysis (EDAX)

HAADF-STEM images were taken by FEI Tecnai F20 instrument equipped with a high brightness field emission electron gun (FEG) operated at 200 kV and a HAADF detector. Prior to the imaging, the Pd/SOMS and Pd/ Al_2O_3 samples were suspended in ethanol and sonicated for 5 min. After obtaining a homogeneous mixture a drop of it was added on a Tedpella, Inc. 200 mesh copper grid sample holder, which was coated with lacey carbon. For identification of Pd particles, EDAX spectra were collected over all the samples.

2.2.5. Static vapor-phase adsorption

Static vapor equilibrium adsorption at $25\text{ }^\circ\text{C}$ were measured over time using Pyris 1 Perkin-Elmer thermo-gravimetric analyzer. A mass of sample was placed on the balance and a neat liquid or solid was added to the sealed analysis chamber to yield a static condition of saturated vapor. Mass was measured every 6 s until equilibrium was reached.

2.2.6. In situ diffuse reflectance infrared fourier transform spectroscopy (DRIFTS)

In situ DRIFTS experiments during temperature programmed desorption (TPD) was performed using a Thermo NICOLET 6700 FTIR spectrometer. The instrument includes a MCT detector operating at liquid nitrogen temperature and a KBr beam splitter. *In situ* experiments were conducted in a Praying Mantis controlled atmosphere reaction chamber in which the samples were loaded. A TCE bubbler at room temperature was used to generate TCE vapors, which were then introduced to the reactor cell using helium as a balance gas. After 1 h of TCE adsorption, the reaction chamber was flushed with helium for 5 min and a spectrum was collected at $25\text{ }^\circ\text{C}$. The temperature was then increased to the next desired set point and another spectrum was collected. The process was repeated up to a temperature of $250\text{ }^\circ\text{C}$.

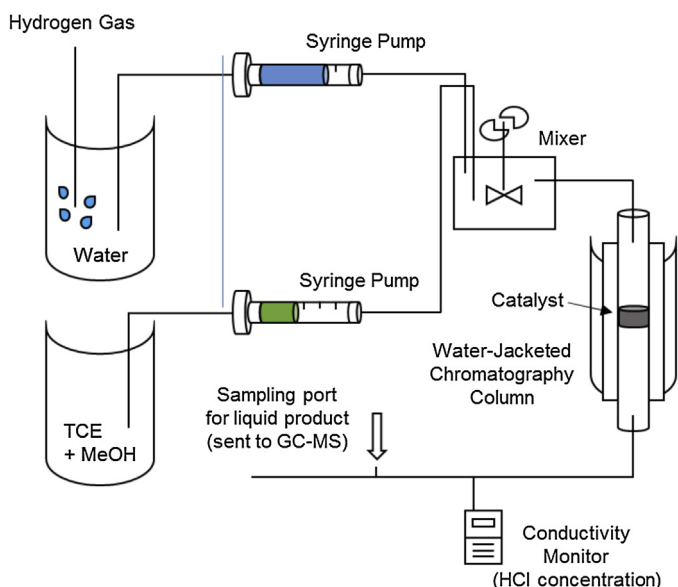


Fig. 2. Diagram of the liquid phase reactor system including a continuous flow of reactants and a fixed bed reactor.

2.2.7. X-ray photoelectron spectroscopy (XPS)

XPS spectra were collected over the Pd/SOMS and Pd/ Al_2O_3 catalysts by using a Kratos AXIS Ultra X-ray photoelectron spectrometer with a monochromatized Al $\text{K}\alpha$ X-ray source operated at 13 kV and 10 mA . The sample was loaded in the chamber using carbon tape and was evacuated overnight. For each sample, a survey scan was taken in order to identify all the elements present on the catalyst surface. After the survey scan, spectra for the specific C 1s, O 1s, Cl 2p, Pd 3d and Si 2p regions were collected. Prior to the data analysis, the charging effect was corrected based on the C 1s binding energy of 284.5 eV . The background subtraction, normalization and peak fitting of the data were performed in CasaXPS software.

2.2.8. Inductively coupled plasma optical emission spectrometry (ICP-OES)

To examine leaching characteristics of the active metal in pre-reduced 1% Pd/ Al_2O_3 and 1% Pd/SOMS, samples 1 M HCl poisoning was conducted by stirring each of the two samples in 40 mL of 0, 0.1 and 1 M HCl solutions for 20 min at RT. The resulting mixture was then filtered to remove all the residual solids. The elemental analysis of Pd in the HCl solution was conducted utilizing a Perkin-Elmer Optima 4300DV ICP-OES.

2.3. Catalytic activity testing

2.3.1. HDC of TCE in the liquid phase

A continuous flow, fixed bed reactor was constructed using a LCC-500 fast flow liquid chromatography system (Pharmacia). A diagram of the reactor system is shown in Fig. 2. All the experiments were based on equal liquid hour space velocity (LHSV = reactant flow rate/reactor volume). The liquid feed consisted of water, TCE, H_2 and methanol. Deionized water was saturated with H_2 by continuously sparging the 4 L source water reservoir. TCE was dissolved in methanol (5.18 mg/mL), to allow rapid dissolution, and introduced to the flow stream by a syringe pump. TCE solution feed rates were either 2.4 mL/h when TCE was limiting or 9.6 mL/hr when the dissolved H_2 was the limiting reagent. A 50–60 Hz mixer upstream of the catalyst bed ensured a homogenous solution. Catalyst was added to a 15 mm diameter water-jacketed chromatography column (GE-Pharmacia) so that the bed thickness remained constant at 4 mm which required 2.0 g of Pd/ Al_2O_3 , 0.40 g of Pd/SOMS, and

0.27 g of pre-swollen Pd/SOMS. Catalyst bed was maintained at 30 °C. Flow rate was 20 mL/min (~40 bed volumes per min).

Reaction progress was monitored by measuring the conductivity of the water in the effluent of the catalytic bed (HCl production) using a Pharmacia Biotech 18-1500 conductivity monitor with 1 Hz data acquisition. In addition, a sampling port was used to collect product stream samples into sealed vials for analysis of chlorinated solvents by headspace gas chromatography-mass spectrometry (GC-MS) using an 6980/5973 instrument (Agilent).

2.3.2. HDC of TCE in the gas phase

The catalytic activity of the 1% Pd/SOMS and 1% Pd/Al₂O₃ in the gas phase for HDC of TCE was measured using a bench-scale fixed-bed flow reactor system. The catalyst was first placed inside a 4 mm-ID quartz reactor using quartz wool plugs to support the catalyst bed. The reactor was then positioned in the center of a furnace (Carbolite, MTF 10/15/130) whose temperature was adjusted by an Omega CSC232 PID temperature controller. The outlet of the reactor was connected to an online gas chromatographer (Shimadzu Scientific 2010) equipped with a Q-bond column and a flame ionization detector (FID) for separation, identification, and quantification of all the products. The inlet stream to the reactor contained 0.7% TCE, excess hydrogen (1:30, TCE-to-hydrogen molar ratio), and nitrogen as the balance gas. The TCE vapors were generated by using a stainless-steel bubbler, which contained pure TCE and which was held at 35 °C using nitrogen as a carrier gas. The effluent gas mixture from the bubbler was then mixed with additional nitrogen and excess hydrogen to obtain 0.7% TCE in feed stream. In order to investigate the effect of water on the catalytic activity of the samples, water was added to the reactant stream. Similar to the TCE, a water bubbler, which was maintained at 35 °C, was to generate water vapor. The total water concentration used in the feed stream was 4%. The HDC of TCE reaction was performed at 50 °C, 100 °C, 150 °C and 200 °C.

All the gas lines (Swagelok) were held at temperatures above 200 °C to prevent any condensation of the reactants and products. Prior to the HDC reaction experiment, the 1% Pd/Al₂O₃ was pre-reduced in-situ by using 5% H₂/He at 400 °C for 1 h. The Pd/SOMS was chemically reduced using NaBH₄. The quantification of the products and reactants was done based on calibration curves that were obtained periodically. The catalytic activity comparison between the two samples was based on equal gas hour space velocity (GHSV).

3. Results and discussion

3.1. Structure of SOMS

SOMS is synthesized using a bis(trimethoxysilyl)benzene (BTEB) silane monomer precursor which contains a benzene ring directly connected to silicon (Fig. 1). The poly-condensation of BTEB during sol-gel synthesis creates a highly cross-linked polymer matrix including covalent linkages between the aryl group and silicon. In a recent study, Edmiston and co-workers [33,34] have examined the effect of various parameters such as the choice of precursor, solvent, catalysts, aging time and silane concentration to investigate the principle behind the swelling behavior. Interestingly, the swelling behavior of SOMS was only obtained by the two precursors that included a covalent bond between the aryl groups connected to the silicon center. Thus, the flexibility of SOMS is possibly correlated to the Si-C-aryl bonds. To obtain a better understanding of the chemical structure of SOMS, two different spectroscopy techniques were used.

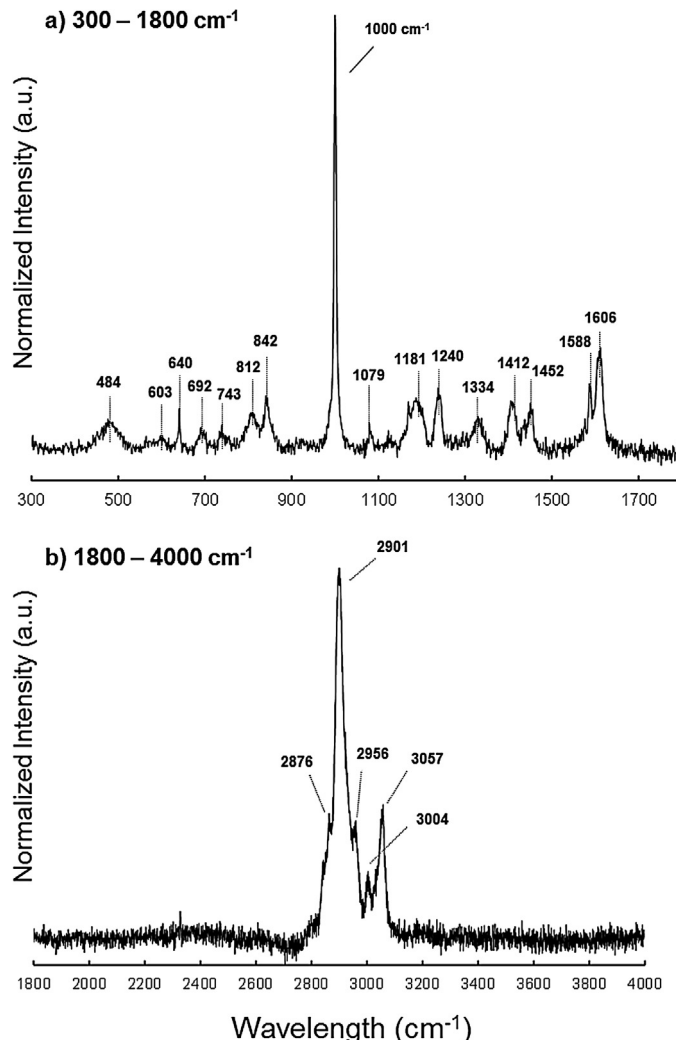


Fig. 3. Raman spectra of SOMS, (a) 300–1800 cm⁻¹ and (b) 1800–4000 cm⁻¹.

3.1.1. Raman spectroscopy

Raman spectrum was collected over the bare SOMS support. Fig. 3(a) shows the spectrum region of 300–1800 cm⁻¹. The band with the strongest intensity at 1000 cm⁻¹ is attributed to mono, 1,3 and 1,3,5 substituted benzenes [38]. This indicates that the aromatic ring originating from the BTEB precursor was stable throughout the synthesis process. The Si-O-Si asymmetric stretching was observed as a sharp feature at 1079 cm⁻¹ [39,40] whereas the Si-O-Si symmetric stretching was assigned to a peak at 640 cm⁻¹ [41,42]. Several other peaks appeared around the lower wavelength region below 1000 cm⁻¹. The bands at 484 and 603 cm⁻¹ are possibly related to three- or four-membered rings of the Si-O-Si symmetric stretching mode, which are typically found in silica Raman spectra [43,44]. However, the intensity of these peaks were much lower. The features for Si-CH₃ appear as a sharp peak at 1240 cm⁻¹ ascribed to the CH₃ symmetric deformation [40]. Peaks at 812 and 842 cm⁻¹ were associated to two methyl groups in Si-(CH₃)₂ binding to the silicon center and the band at 1412 cm⁻¹ was attributed to the asymmetric stretching of the CH₃ species [40]. It is likely that Si-CH₂-R bonds are present in the structure. The 692 and 743 cm⁻¹ bands were assigned to the rocking vibration of CH₂ [40]. Si-O-CH₃ bonds were also identified as a strong peak at 1181 cm⁻¹ [40]. The CH₃ symmetric stretching in C-CH₃ group were also seen at 1334 cm⁻¹ [40]. The higher wavenumber range above 1400 cm⁻¹ are mostly due to adsorption of aromatic groups.

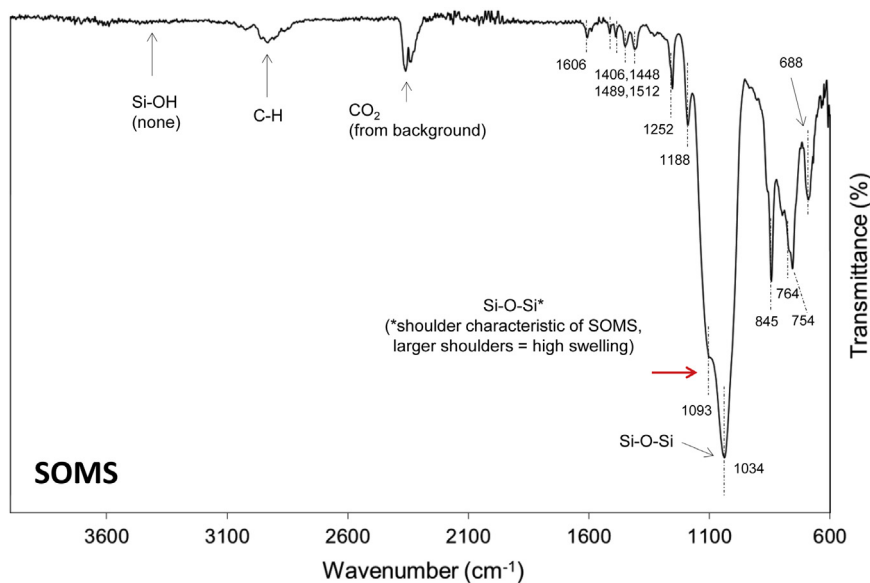


Fig. 4. IR spectra of SOMS.

The 1452, 1588 and 1606 cm⁻¹ peaks are due to aromatic rings with different substituents [40,45].

The high wavenumber-region of the spectrum led to similar observations as seen in Fig. 3(b). The adsorption due to C—H stretching in aromatic rings were observed at 3004 and 3057 cm⁻¹ [40,45]. The peaks at 2956, 2901 and 2876 cm⁻¹ are attributed to C—H vibration in CH₃ or CH₂ groups of aliphatic compounds [40,45], or Si—O—CH₃ groups [46].

3.1.2. IR spectroscopy

The structural characteristics of the SOMS materials were also examined using IR spectroscopy (Fig. 4). The two overlapping peaks at 1034 and 1093 cm⁻¹ indicate Si—O—Si stretching [47]. The shoulder of Si—O—Si band is characteristic of SOMS and due to longitudinal-optic (LO)—transverse-optical (TO) splitting of the vibrational modes. LO—TO splitting has been attributed to long range coupling of Coulomb interactions [48–50]. Specifically, the antisymmetric stretching LO₃ (1188)—TO₃ (1093) cm⁻¹ bands observed in SOMS are likely explained as scattering in larger pore structures [51].

The Si—OH groups were not observed, i.e. showing no notable peaks around the 3000–3600 cm⁻¹ or 950 cm⁻¹ regions [47]. This is due to the Si—OH groups being capped by treatment with chlorotrimethylsilane in the synthesis of SOMS [33] leading to O—Si—(CH₃)₃ groups which were detected by Raman and observed in the IR by three distinctive peaks at 764, 845 and 1252 cm⁻¹ [47]. Multiple bands associated with the aromatic ring were shown in the spectrum. Two strong peaks at 688 and 754 cm⁻¹ exhibit features that correspond to out-of-plane C—H bending or wagging vibrations of mono and meta substituted benzenes [47,52]. The in-plane C—H bending was observed around 1400–1700 cm⁻¹ region. The five peaks at 1406, 1448, 1489, 1512, and 1606 cm⁻¹ can be related to a combination of mono, ortho, meta and para substituted benzenes of the SOMS structure [52].

3.2. Thermal stability of SOMS

SOMS is an organosilica-based material which consists of a crosslinked network. It is expected that under extreme thermal treatment, the structure of SOMS collapses due to decomposition of the organic groups, resulting in the loss of the swelling capability and hydrophobicity. Hence, a TPO experiment was conducted

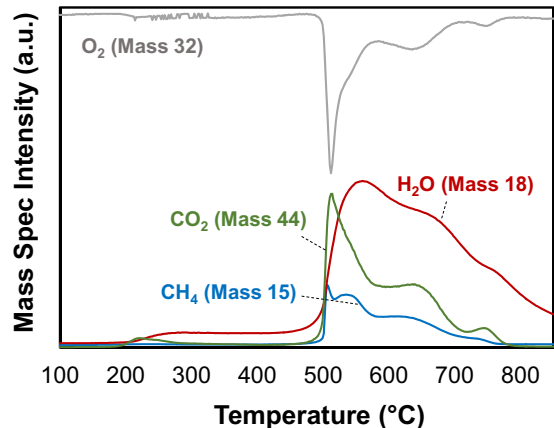


Fig. 5. Temperature-programmed oxidation (TPO) profiles showing decomposition of SOMS at high temperatures (>450 °C).

to determine an accurate decomposition temperature of the SOMS material. As shown in Fig. 5, a significant oxygen consumption feature was observed around 500 °C, simultaneously producing a large amount of CO₂. This clearly shows that the decomposition of SOMS with C—C bond cleavage. Some amount of H₂O and CH₄ was also detected as products. Interestingly, the swelling property and hydrophobicity in the post-TPO SOMS sample was still present (data not shown). However, the degree of physical volume expansion was significantly reduced compared to the fresh SOMS support. The weak thermal stability of the SOMS support limited its utilization in the H₂ pre-reduction process, which requires high temperatures. Thus, for this study, all of the Pd/SOMS samples were pre-reduced using NaBH₄ at room temperature.

3.3. Surface area, pore size and pore volume

The nitrogen isotherms of the samples were collected using an ASAP 2020 instrument to obtain BET surface area, BJH pore volume and averaged pore diameter. The calculated values are shown in Table 1. The impregnation of Pd on the SOMS support showed reduction in surface area, pore volume and averaged pore diameter. This is likely attributed to the filling/blockage of the pores of the

Table 1

BET Surface area, pore volume and average pore diameter of SOMS, 1% Pd/SOMS and 1% Pd/Al₂O₃ catalysts.

	Surface Area (m ² /g)	Pore Volume (cm ³ /g)	Averaged Pore Diameter (Å)
SOMS	493	1.03	84
1% Pd/SOMS	479	0.56	47
1% Pd/Al ₂ O ₃	156	0.85	217

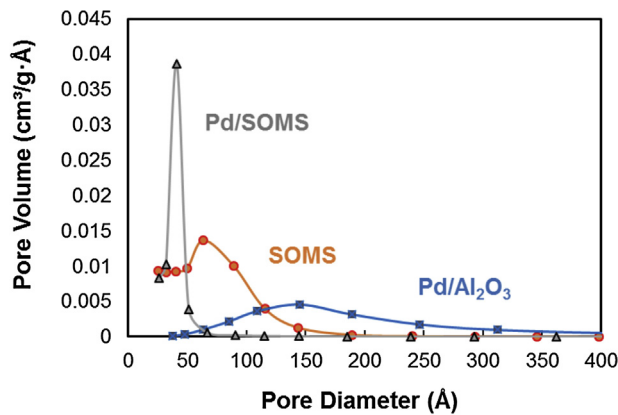


Fig. 6. BJH Pore size distribution of SOMS, 1% Pd/SOMS and 1% Pd/Al₂O₃.

SOMS support by Pd particles. The surface area of 1% Pd/SOMS was higher than that of the 1% Pd/Al₂O₃ commercial catalyst. However, 1% Pd/Al₂O₃ exhibited a higher pore volume and a higher average pore. The BJH pore size distributions are shown in Fig. 6. As it can be seen, a significant decrease in number of pores of 50–200 Å over the SOMS support was observed after the Pd impregnation process. For Pd/SOMS sample, most of the pores detected were close to 50 Å (mesopores) whereas a wide pore size distribution in the range of 50–400 Å was obtained for Pd/Al₂O₃.

All the SOMS and 1% Pd/SOMS samples tested here were in their closed state, i.e., before any physical expansion of the material has taken place. The open-state of these samples were not subjected for the analysis due to the degassing and analysis conditions. However, it should be noted that the surface area and pore volume of the open-SOMS and open-1% Pd/SOMS are expected to be significantly greater compared to the closed state of the two samples. This is attributed to the generation of the inner surface area during swelling of the samples, hence, the actual surface area, pore volume and pore size would be higher under reaction conditions.

3.4. Hydrophobicity and adsorption capacity of 1% Pd/SOMS vs 1% Pd/Al₂O₃

Adsorption capacity of SOMS for different organics (acetone, heptane, methanol, TCE, and benzene) was measured at room temperature using the static vapor adsorption technique and compared to that for water vapor. The term adsorption here refers to physisorption and involves pore filling. The mass intake profiles for these organics and for water are shown in Fig. 7. The results indicate SOMS had adsorptive capacity for organic vapors between 60 and 100% w/w. Capacity after 120 min exposure time was generally non-selective across all organic vapors. In contrast, water vapor adsorption was <7% w/w, verifying the high hydrophobicity of SOMS.

In an earlier study by Edmiston and co-workers [35], SOMS was shown to be capable of adsorbing both polar and non-polar organic substances dissolved in aqueous phase. The study reported adsorption capacity for several organics, including PCE, TCE, toluene, methyl t-butyl ether (MTBE), acetone, naphthalene, and 1-butanol.

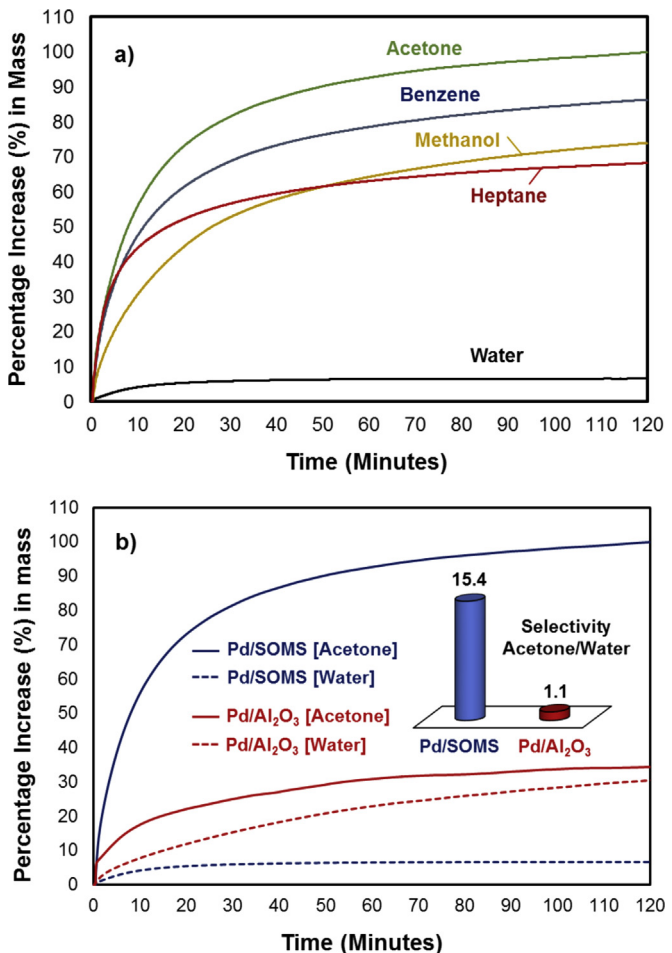


Fig. 7. (a) Adsorption of different organic groups on 1% Pd/SOMS, (b) Adsorption of water and acetone on 1% Pd/SOMS and 1% Pd/Al₂O₃ catalysts.

Especially several compounds that are very relevant to water contamination problem such as PCE, TCE and toluene were adsorbed from water by SOMS at extraction levels of 92% or above [35].

Fig. 7(b) shows a comparison of 1% Pd/SOMS and 1% Pd/Al₂O₃ catalysts and their adsorption uptake capacities for gas-phase acetone and water. The adsorption selectivity of acetone to water, i.e., ratio of the weight of acetone adsorbed to that of water adsorbed, was seen to be much higher for Pd/SOMS than it was for Pd/Al₂O₃ as seen in the inset. It also shows that SOMS is much more hydrophobic than Al₂O₃ and the Pd impregnation of the reduction step with NaBH₄ does not change the hydrophobic nature of this material.

3.5. HDC of TCE in liquid phase

3.5.1. Pd/SOMS vs. Pd/Al₂O₃

The catalytic activity of Pd/SOMS and Pd/Al₂O₃ was investigated in liquid phase for HDC of TCE using a continuous flow reactor system where the aqueous phase reactant mixture (TCE + water), was introduced into a fixed catalyst bed. A thin bed of supported catalyst was used to give a short residence time to better assess the kinetics of the HDC reaction. The effluent stream from the reactor was monitored by a conductivity detector, where the concentration of HCl was directly correlated to hydrodechlorination activity of the catalyst. These experiments were conducted in three parts: (i) with 180 μM TCE (24 ppm) in the feed, i.e., TCE is the limiting reactant; (ii) with 320 μM TCE (42 ppm) in the feed, i.e., H₂ is the limiting reactant; (iii) ending with TCE-free feed. In all three parts

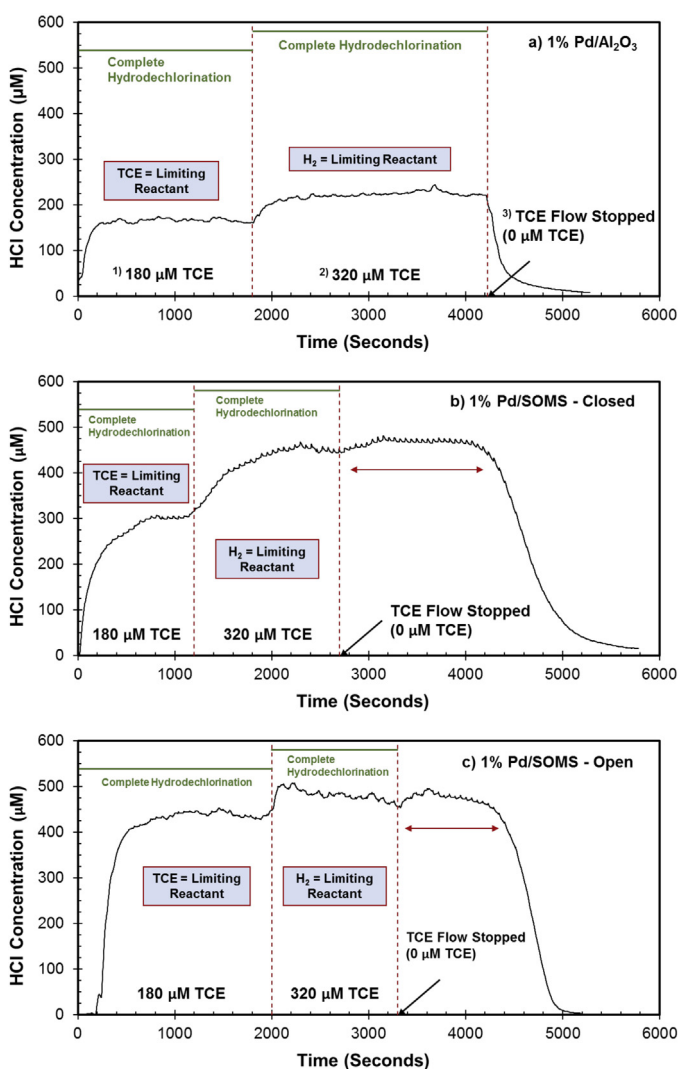


Fig. 8. Catalytic activity data for (a) 1% Pd/Al₂O₃, (b) 1% Pd/SOMS-closed and (c) 1% Pd/SOMS-open for HDC of TCE in continuous flow liquid-phase reactor.

of the experiment, H₂ concentration in the feed was kept constant at 775 μM.

Fig. 8(a) shows the liquid-phase hydrodechlorination of TCE over 1% Pd/Al₂O₃ at three different TCE concentrations. The green bar at the top of each section indicates the theoretical HCl concentration when complete hydrodechlorination of TCE is achieved. When 180 μM of TCE was introduced to the reactor, after a transient period of 290 s, a steady-state percent hydrodechlorination (%HDC) of around 35% was obtained over the 1% Pd/Al₂O₃ catalyst. Here %HDC is defined as $100 \times (\text{moles of HCl produced}) / (3 \times \text{mol of TCE fed})$. The %HDC slightly increased to 40% as TCE concentration was increased to 320 μM. As expected, when there was no TCE in the reactor feed, as shown in the third section of the graph, the HCl concentration in the effluent quickly dropped to 0 μM. Water collected during the steady-state period ($t = 1200$ s) was tested for the presence of chlorinated solvents by GC-MS. At steady state, TCE ($C_{\text{out}}/C_{\text{in}} = 0.25$), and a range of partially dechlorinated compounds including dichloroethylene, and vinyl chloride were detected in the effluent, supporting incomplete HDC reaction as indicated by sub-stoichiometric HCl production.

Pd/SOMS catalyst showed a different performance from Pd/Al₂O₃ (Fig. 8(b)). For Pd/SOMS, the transient period was much longer (850 s) as the HCl concentration gradually rose to the steady-state value. The hydrodechlorination activity was higher than that

of Pd/Al₂O₃, with 63 and 79% HDC conversion levels, for 180 μM and 320 μM of TCE inlet concentrations, respectively. It should be noted that the Pd/SOMS initially loaded into the bed was in the closed (unswollen) state. In other words, the catalyst was not pretreated with an organic solvent (ethanol), which would swell the pores prior to the reaction. The collapsed initial pore architecture may account for the slow approach to steady-state and the long transient period, during which the pores of the SOMS support are expected to be filled by TCE adsorption. In other words, during this period TCE would be concentrating inside the pores. Another interesting observation from these experiments is that HCl was detected in the effluent for an extended time (1500 s) after discontinuing TCE addition to the deionized feed water. Continued HCl production can be explained by the reaction continuing from the reservoir of adsorbed TCE as well as desorption of retained HCl. The amount of chlorinated solvents in the reactor effluent was measured at $t = 1000, 2500, 5000$ s ($[TCE]_{\text{in}} = 180, 320$, and 0 μM, respectively). At all-time points, the amount of TCE in the reactor effluent water was undetectable by GC-MS. An amount of vinyl chloride approximately 10% of the TCE effluent concentration was detected when TCE was in stoichiometric excess of H₂ ($t = 2500$ s). Ethane was detected at all-time points, but was not quantified.

The result shown for Pd/SOMS is surprising and significant as it was deduced that the SOMS support itself has a large adsorptive capacity for TCE, resulting in a high concentration of the reactant inside the pores and the ability to "buffer" TCE input loads. An amount of vinyl chloride likely escapes during the elevated TCE input since the vinyl chloride is more soluble in water and likely builds up in the pores due to H₂ starvation. The high storage capacity is a unique feature which is facilitated by the swelling and adsorptive characteristics of SOMS. The hydrophobic nature of SOMS, which repels water, but allows adsorption of organics inside the pores appears to improve the kinetics, since local concentration of TCE inside the pores, i.e., in the vicinity of the active sites would be much higher than in the bulk of the liquid.

To examine the effect of volumetrically expanding the pores, Pd/SOMS was first pretreated with ethanol in order to reach its maximum swollen state to make the catalyst pores fully opened prior to reaction. The Pd/SOMS-open was then tested for HDC of TCE (Fig. 8(c)). When the pores are volumetrically expanded by ethanol pre-treatment, a significant increase in the HDC conversion was obtained over the 1% Pd/SOMS-open compared to 1% Pd/SOMS-closed and 1% Pd/Al₂O₃ catalysts in both TCE feed concentrations. The HCl concentration obtained with 180 μM TCE feed reached a maximum value at 94% of HDC conversion. This is 31% greater compared to Pd/SOMS-closed sample. In the second region where 42 ppm of TCE feed was utilized, %HDC reached 84%. An important observation is that the approach to steady-state i.e., transient period was much shorter (420 s) for the Pd/SOMS-open sample since the pores were already fully opened when the feed was introduced and the TCE could concentrate inside the pores much faster. Similarly, the production of HCl was continued for a shorter time (900 s) after addition of TCE to reactant stream was stopped, compared to the Pd/SOMS-closed. This is likely due to the higher conversion rate of the reactant, which results in a faster depletion rate of the TCE "stored" in the pores. Chlorinated solvent concentrations in the effluent were measured at $t = 1800, 3000, 4500$ s. TCE and all partially dechlorinated compounds were undetectable at 1800 s ($[TCE]_{\text{in}} = 180$ μM) and 4500 s ($[TCE]_{\text{in}} = 0$ μM, post addition). When TCE was in excess ($t = 3000$ s) a small amount of TCE ($C_{\text{out}}/C_{\text{in}} = 0.02$) and vinyl chloride were detected suggesting the open state-SOMS has capability of adsorbing TCE.

The faster kinetics due to concentration of TCE inside the pores is seen more clearly when the results obtained over Pd/Al₂O₃ and Pd/SOMS (both open and closed) are compared. In these experiments, the feed flow rate and concentration were kept constant,

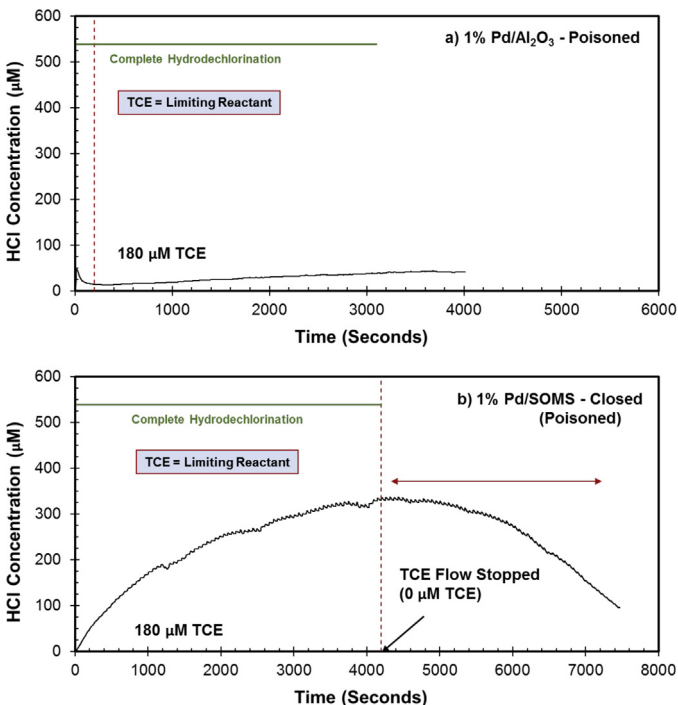


Fig. 9. Catalytic activity data for (a) Li₂S-poisoned 1% Pd/Al₂O₃ and (b) Li₂S-poisoned 1% Pd/SOMS – closed for HDC of TCE in continuous flow liquid-phase reactor.

but the amount of Pd/Al₂O₃ in the reactor was more than 5 and 7 times that of the Pd/SOMS and Pd/SOMS-open, respectively. This result shows that the high hydrodechlorination rates obtained over Pd/SOMS (both open and closed) cannot be explained by their higher surface areas.

It should be noted that the pH of the reactant solution could affect the catalytic activity as well as stability. It is also possible that the acidity of the reactant solution may influence the degree of swelling of the Pd/SOMS catalyst. Thus, a comparison study of the catalytic activity of Pd/Al₂O₃ and Pd/SOMS (both open and closed) in basic media would be informative and is under progress.

3.5.2. Catalytic activity of Li₂S poisoned Pd/SOMS and Pd/Al₂O₃

Another advantageous aspect of SOMS material is the hydrophobicity which makes the Pd/SOMS catalyst considerably resistant to ionic poisons. Various ionic poisons, which exist in groundwater, decrease the performance of the catalyst. Among them, several studies have shown that sulfur containing groups have a significant impact on the stability of Pd-based catalysts used for HDC of TCE. In this study, lithium sulfide (Li₂S) was used as a model poison compound in order to investigate the effectiveness of the hydrophobic SOMS support in protecting the Pd active sites from poisoning.

HDC activity was measured for 1% Pd/SOMS was poisoned ex-situ by soaking in a solution containing 5 ppm of Li₂S and 1 ppm Na₂CO₃ for 1 h. As a comparison, 1% Pd/Al₂O₃ was also poisoned using Li₂S under the same conditions. Fig. 9(a) and (b) shows the catalytic activity data collected over the two Li₂S-poisoned-samples for HDC of TCE. It is clear that a complete deactivation was observed for the Pd/Al₂O₃ catalyst after poisoning whereas Pd/SOMS remained partially active.

As previously mentioned, the observed initial time lag over Pd/SOMS catalyst was ascribed to the adsorption time of TCE into the pores of the support. However, compared to the fresh 1% Pd/SOMS-closed, the approach to steady state was slower (850 s vs 4100 s), i.e., more time was required to reach to the same conversion at steady-state for the poisoned sample. The vapor phase adsorp-

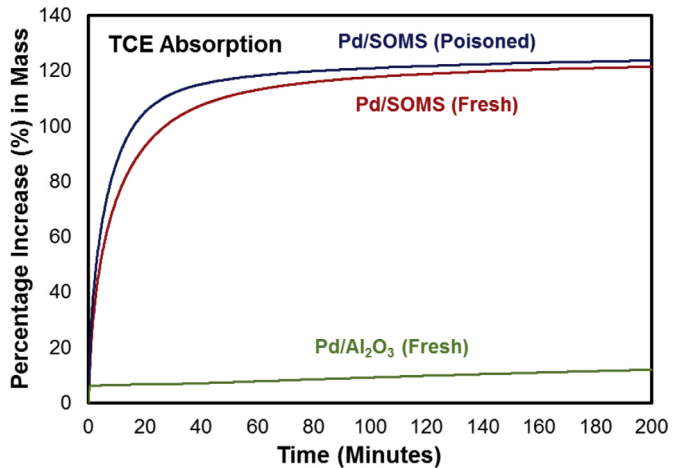


Fig. 10. TCE adsorption profile for fresh and Li₂S-poisoned 1% Pd/SOMS-closed and fresh 1% Pd/Al₂O₃ catalysts.

tion of TCE to Pd/Al₂O₃ and Pd/SOMS before and after poisoning was measured (Fig. 10). Similar to other organic vapors, Pd/SOMS has a high adsorption capacity for TCE, 125% w/w, which is 10× more than the amount of TCE adsorbed by Pd/Al₂O₃. Exposure of Pd/SOMS to Li₂S had no deleterious effect on the TCE adsorption, indicating that the slower activity is due to changes in catalyst activity and not the affinity of the sorbent support. The slower rise time is likely due to poisoning of Pd particles near the surface of the SOMS support whereas particles deeper in the hydrophobic matrix appear to be protected from sulfide. TCE must adsorb further into the pores to reach active catalyst. A longer time-lag was also seen when the TCE flow was stopped in which more than 50 min was spent to release all the adsorbed TCE molecules. These data indicate that the SOMS matrix can exclude anionic poisons, especially if the particles are embedded in the matrix where aqueous solutions cannot penetrate.

To further investigate TCE adsorption behavior over the Pd/SOMS and Pd/Al₂O₃ catalysts, *in situ* DRIFTS experiments were performed during TPD. As seen in Fig. 11, adsorption of TCE on both catalysts was observed, as manifested through the bands at 781, 841 and 940 cm⁻¹ for Pd/SOMS and 783, 845 and 943 cm⁻¹ for Pd/Al₂O₃ catalysts [53]. These bands are assigned to C–Cl (781 and 940 cm⁻¹) and C–H bending (841 cm⁻¹) vibrations of the TCE molecules that were maintained even at elevated temperatures [53]. The 1581 and 1556 cm⁻¹ peaks are associated to C=C bond of TCE [53], and possibly related to the molecularly adsorbed TCE on the catalyst surface.

There are two major differences between the spectra of Pd/SOMS and Pd/Al₂O₃. One is the band at 1640 cm⁻¹, which is not seen over Pd/SOMS, but is present in Pd/Al₂O₃ spectrum with significant intensity. This band can be assigned to adsorbed water on the catalyst surface [54]. These results exhibit the strong hydrophobicity of the Pd/SOMS sample compared to Pd/Al₂O₃. Another difference is that the bands 1450 and 1550 cm⁻¹, which were observed over Pd/Al₂O₃ catalyst above 100 °C, and, which can be assigned to carboxylate-type species, were not seen in the spectra of Pd/SOMS [55]. Chintawar and Greene performed a similar study using Cr-Y catalyst and reported monochloroacetate (CH₂Cl⁻COO⁻) as an intermediate compound [56]. The formation of monochloroacetate indicates participation of surface oxygen of Al₂O₃ support during TCE adsorption. The lack of similar features over the Pd/SOMS spectra may be due weaker bonds to the surface which may result in short-lived surface species. It is also possible that adsorption of TCE may go through a different intermediate over Pd/SOMS.

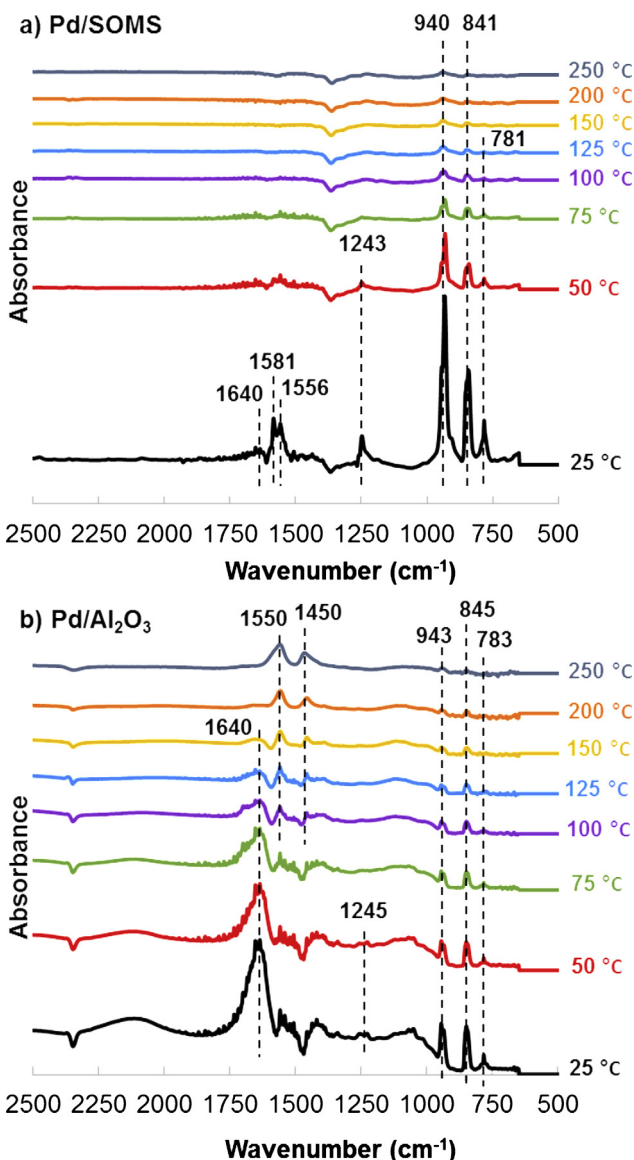


Fig. 11. TCE TPD *in situ* DRIFTS results over Pd/SOMS and Pd/Al₂O₃ catalysts.

3.6. Pd leaching with HCl

Catalyst deactivation due to HCl was investigated since HCl is a potential inhibitory product of the HDC of TCE reaction. The chloride ions interact with Pd active sites, they may affect the oxidation state of Pd, or facilitate the carbon deposition on the catalyst surface [15,25]. Besides, Pd leaching has been reported due to decrease in pH during hydrodechlorination reactions [32,57]. Similar to the previous sulfur poisoning studies, it was expected that the hydrophobicity of the Pd/SOMS catalyst may provide some protection by repelling the Cl⁻ ions. However, it is possible that the resistance to chloride may decay when high concentration of HCl is used. To allow comparison, both Pd/SOMS and Pd/Al₂O₃ were treated *ex-situ* using 1 M HCl and characterized using XPS, STEM/EDAX and ICP-OES techniques.

3.6.1. XPS results

Fig. 12(a) shows the Cl 2p spectra collected over the HCl-treated Pd/SOMS and Pd/Al₂O₃ samples. The high intensity of the peak validates that Cl ions were adsorbed on the Pd/Al₂O₃ catalyst surface in contrast to Pd/SOMS sample where no Cl signal was detected.

Table 2

ICP-OES results showing percentages of Pd leached from 1% Pd/Al₂O₃ and 1% Pd/SOMS samples after they were exposed to different concentrations of HCl.

Pd leached (%)	0 M HCl	0.1 M HCl	1 M HCl
	1%Pd/Al ₂ O ₃	74.4	>99
1%Pd/SOMS	0	1.6	6.4

Regarding the Si 2p spectra, no oxidation state change of the Si was observed. The peak at 102.5 eV indicates that Si species consist lower oxidation state (+1 and +2) including features of SiC peak [58–60]. The spectra for Pd 3d for Pd/Al₂O₃ in Fig. 12(c) were deconvoluted in order to perform quantification of the oxidation state of Pd particles and to understand the change in oxidation states due to HCl treatment. The peak assignments for Pd⁰ and Pd²⁺ were determined based on the literature. [61–63]. The constraints used in fitting the spectra were that the ratio of the intensities of 3d_{3/2} and 3d_{5/2} was 2:3 and the two peaks were 5.26 eV apart from each other. Since the majority of the Pd particles were located inside the SOMS structure, no Pd was observed for Pd/SOMS (data not shown). However, using the same Pd loading, two distinctive peaks were found in the Pd 3d spectra over the pre-reduced Pd/Al₂O₃ catalyst. These results demonstrate that the Pd is embedded in the SOMS support. The effect of HCl treatment on the oxidation state of Pd on the Al₂O₃ support was apparent where a significant decrease in Pd signal intensity was observed due to Pd leaching. Furthermore, the oxidation state of Pd was increased from 0.12 (pre-reduced) to 1.98 after HCl treatment. This may be attributed to the formation of PdCl₃⁻ and PdCl₄²⁻ complexes, which indirectly affect the change of oxidation state from Pd⁰ to Pd²⁺ by stabilizing Pd in the higher oxidation state [25].

3.6.2. STEM/EDAX and ICP-OES results

STEM and TEM images were taken to observe the particle size and Pd dispersion on SOMS and Al₂O₃ supports. Fig. 13(a) presents STEM images of the fresh 1% Pd/SOMS where white dots represent Pd metals. The Pd metal particles are not homogeneously dispersed on the SOMS support. The particles size varies from the 0–30 nm range. In some areas, Pd particles were seen to agglomerate forming aggregates. Heterogeneity may be due to non-uniform Pd distribution post-drying and/or the chemical reduction process where BH₄⁻ must penetrate the pores to reduce Pd²⁺. In contrast to Pd/SOMS, the fresh 1% Pd/Al₂O₃ catalyst (Fig. 13(b)), exhibits a uniform dispersion of Pd metal with a very narrow particle size range of 1–5 nm. Particle size histograms of the images are shown in Fig. 14.

STEM images and EDAX spectra were obtained over the HCl-treated Pd/Al₂O₃ catalysts. After the 1 M HCl treatment, most of the Pd particles were leached from the Al₂O₃ support as it is shown in the EDAX spectra which no longer displays a Pd peak (Fig. 13(d)). On the other hand, most of the Pd metal was still present in the HCl-treated Pd/SOMS sample (Fig. 13(c)). These results show that the hydrophobicity of the SOMS support plays an important role in protecting the Pd particles from chloride ions.

ICP-OES experiment was carried out to quantify the Pd leaching as well as to compare the chloride resistance of the Pd/SOMS and Pd/Al₂O₃ catalysts. The concentration of the Pd in the filtered solution (post-treatment) was acquired and compared to the original amount of Pd (1%). Based on these measurements, the percentage of Pd leaching was calculated and are shown in Table 2. Results from a control experiment where the catalysts were soaked in water only are also included to isolate the degradation effect due to HCl. As it can be seen, no Pd leaching was observed using the 0 M HCl (pure water). When the HCl concentration was increased to 0.1 M, 74.4% of Pd leached out to the HCl solution from the Al₂O₃ support in

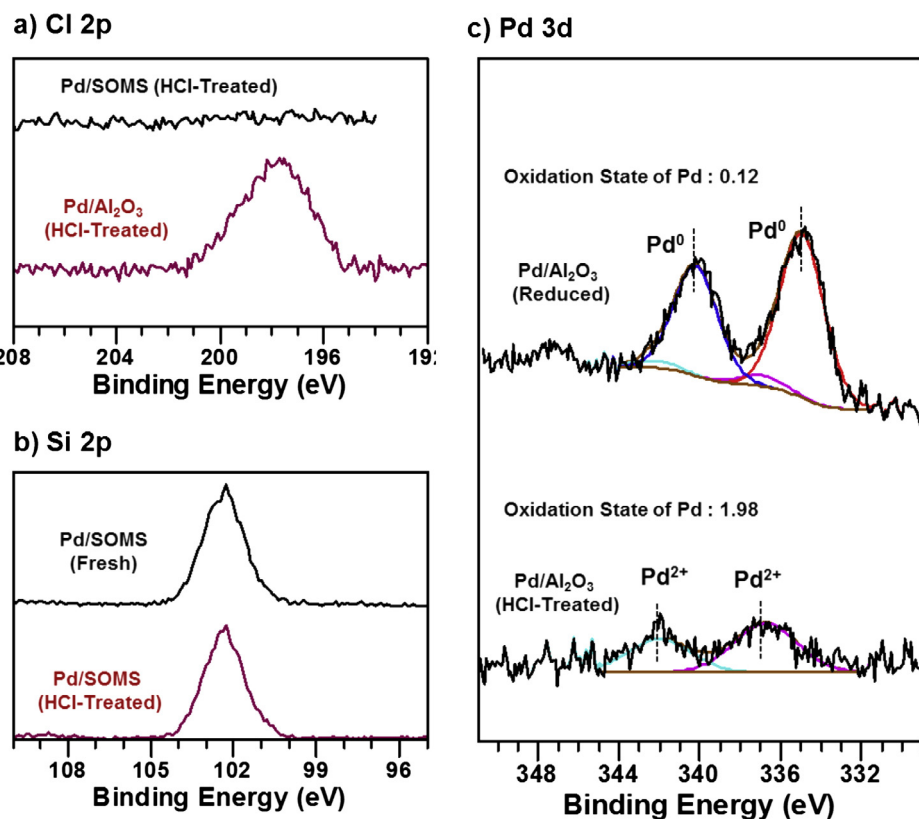


Fig. 12. XPS spectra collected over fresh and HCl-treated 1% Pd/SOMS and 1% Pd/Al₂O₃ catalysts: (a) Cl 2p, (b) Si 2p and (c) Pd 3d.

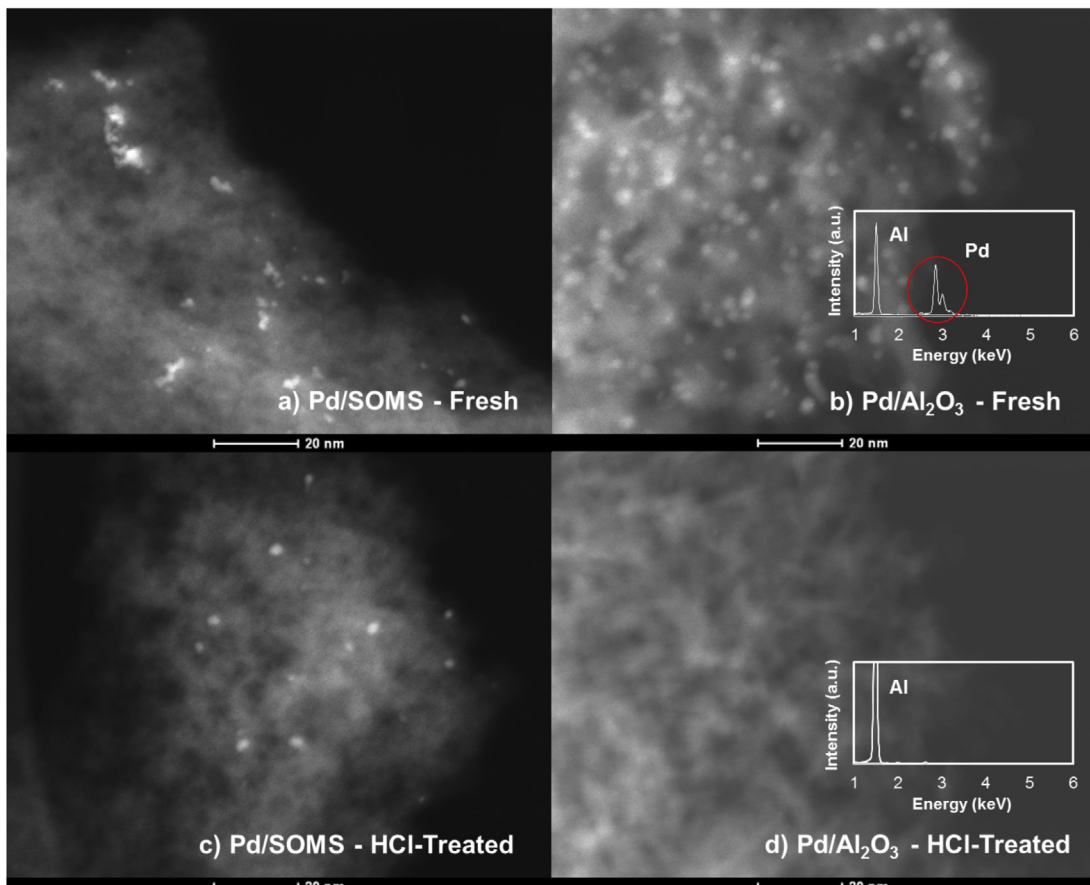


Fig. 13. STEM images of fresh and HCl-treated Pd/SOMS and Pd/Al₂O₃ catalysts.

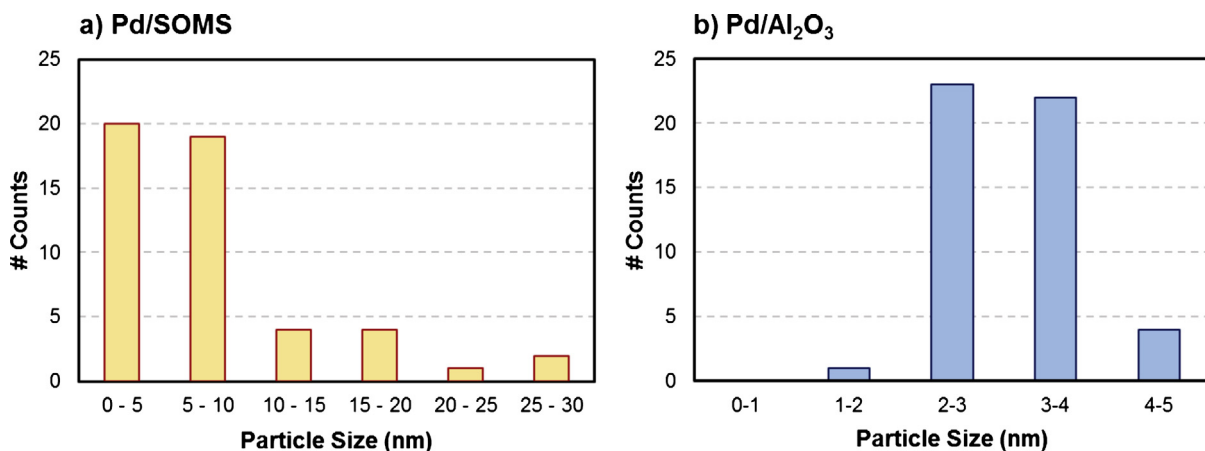


Fig. 14. Particle Size Distribution Histogram for Pd/SOMS and Pd/Al₂O₃ catalysts.

contrary to the Pd/SOMS in which only 1.6% of Pd was leached. At 1 M HCl concentration, all the Pd particles were removed from the Al₂O₃ support as opposed to 6.4% of Pd/SOMS. These results show that the Pd sites over Pd/SOMS are better protected against leaching compared to Pd/Al₂O₃.

3.7. HDC of TCE in the gas phase

In the gas phase, the degree of TCE adsorption by SOMS is much smaller and slower than it is in the liquid phase. Part of this is also due to the higher temperatures used in the gas-phase experiments. As mentioned earlier, the pore-opening process may play an important role for obtaining high catalytic activity since it impacts the accessibility of the Pd active sites and facilitates the concentration of the reactant (TCE) near the active sites (and potentially allowing HCl egress). Fig. 15 shows a comparison of the TCE conversion on the Pd/SOMS and Pd/Al₂O₃ catalysts. In fresh form, 1% Pd/Al₂O₃ sample exhibited significantly higher catalytic performance at all temperatures tested compared to Pd/SOMS (fresh). The difference in catalytic activity of the Pd/SOMS between liquid and gas phase suggests that opening of the pores in SOMS is a key to its superior catalytic performance in the liquid phase HDC of TCE. The fact that Pd is embedded in SOMS helps the kinetics (including protection from anionic poisons), but may lead to a barrier to activity unless there is sufficient adsorption of TCE inside the pores.

The samples treated by 1 M HCl were also tested for gas-phase HDC of TCE. Due to strong Pd leaching over the Pd/Al₂O₃ catalyst, no conversion of TCE was observed. On the other hand, although the TCE conversion is low, there was almost no difference in terms of the catalytic activity between the fresh and HCl-treated Pd/SOMS. Fig. 15(c) shows the percent loss in TCE conversion over the two samples at 50, 100 and 150, 200 °C. These results are significant in reiterating the importance of the pore architecture in SOMS as well as its ability to protect the Pd sites from leaching.

Lastly, the effect of water on the hydrodechlorination activity of Pd/Al₂O₃ and Pd/SOMS was examined, by adding water to the reactant stream. In the presence of water vapor (4%), significant decrease in TCE conversions were observed over the Pd/Al₂O₃ catalyst in comparison with the case when the feed was water-free. There appears to be a strong inhibition effect with water over Pd/Al₂O₃.

In contrast, no decrease in TCE conversions were observed for Pd/SOMS sample with water. This indicates that the strong hydrophobicity of the SOMS support plays an important role for alleviating the water inhibition effect. Fig. 16(c) indicates the percent loss in TCE conversion in the presence of water in the TCE reactant stream. Interestingly, when the reaction temperature was

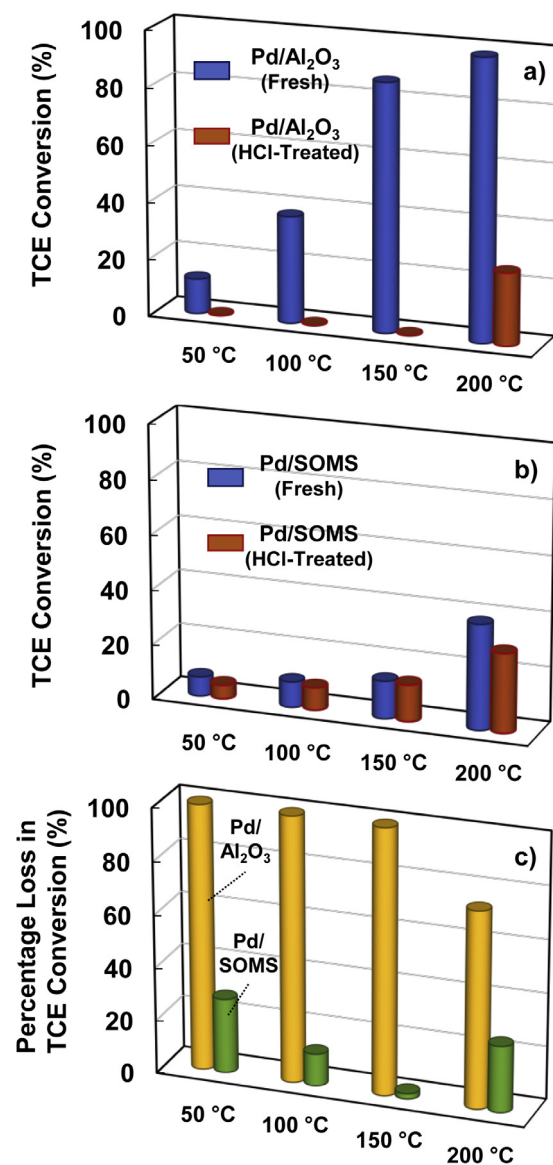


Fig. 15. Catalytic activity data for fresh and HCl-treated (a) 1% Pd/Al₂O₃ and (b) 1%Pd/SOMS samples for HDC of TCE in continuous flow gas-phase reactor, (c) percentage loss in TCE conversion due to HCl treatment.

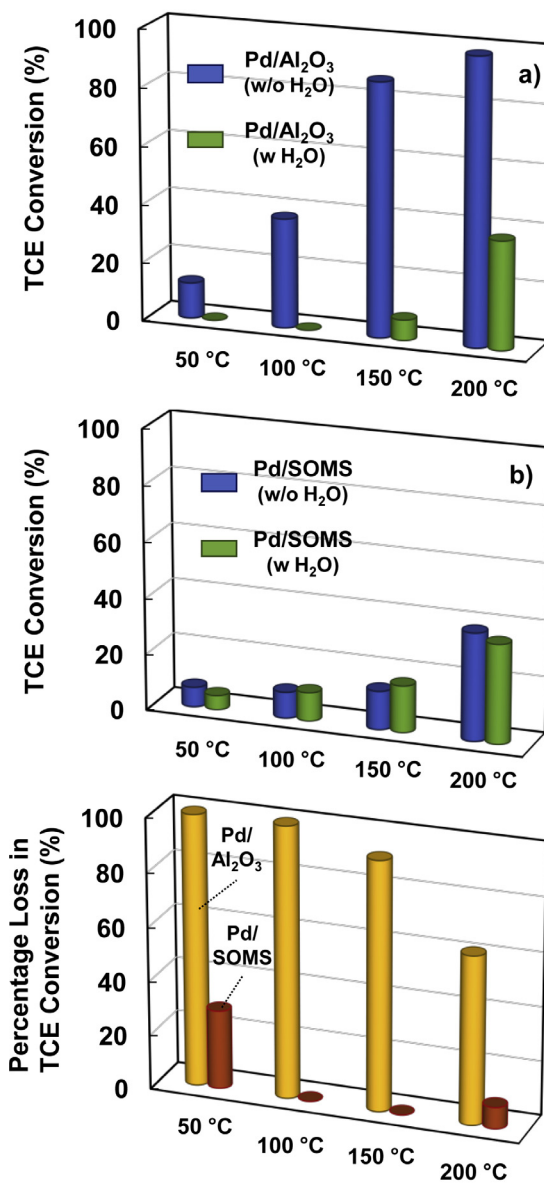


Fig. 16. Catalytic activity data for (a) 1% Pd/Al₂O₃ and (b) 1%Pd/SOMS for HDC of TCE in the presence/absence of water in continuous flow gas-phase reactor, (c) percentage loss in TCE conversion due to water in the feed.

increased to 200 °C, Pd/Al₂O₃ showed better catalytic performance compared to Pd/SOMS in the presence of water. This is likely due to a decrease in the hydrophobicity of the SOMS at higher temperatures. When the%HDC values were compared (not shown), very similar trends were observed in all cases.

4. Conclusions

Swellable organically-modified silica was shown to be a promising support for catalysts used for catalytic treatment of water contaminated with chlorinated hydrocarbons, specifically TCE. Both the swelling capability of SOMS and its high hydrophobicity play a role in improving the kinetics of hydrodechlorination of the reaction, by concentrating the organic contaminants inside the pores in the close vicinity of the pores. Pd catalysts supported on SOMS showed a higher HDC activity in the liquid phase compared to Pd/Al₂O₃ catalysts. However, in the gas phase, Pd/SOMS was less active than Pd/Al₂O₃. This was attributed to a lesser degree of swelling of the Pd/SOMS catalyst in the gas phase. Pd/SOMS cata-

lysts were also shown to be more resistant to deactivation by sulfur compounds or chloride ions than those supported on alumina. Pd species inside the pores of the SOMS support were also shown to be protected against poisoning and leaching in lower pHs. This study demonstrates the potential of these materials as catalyst scaffolds in many applications for catalytic water treatment.

Acknowledgements

The financial support for this work was provided by the National Science Foundation through the Grant CBET-1436729. The authors also acknowledge partial support provided by the Ohio Coal Research Consortium. Authors note the efforts of Allison Curtze and Deanna Pickett at The College of Wooster in conducting supporting experiments.

References

- [1] R.E. Doherty, Environ. Forensics 1 (2000) 69–81.
- [2] M.J. Moran, Occurrence and Implications of Selected Chlorinated Solvents in Ground Water and Source Water in the United States and in Drinking Water in 12 Northeast and Mid-Atlantic States, 1993–2002, 2005, pp. i–ix, 1–70.
- [3] E.P.A. U.S., Occurrence Estimation Methodology and Occurrence Findings Report of the Six-year Review of Existing National Primary Drinking Water Regulations, 2003 (Washington, DC).
- [4] E.P.A. U.S., Toxicological Review of Trichloroethylene In Support of Summary Information on the Integrated Risk Information System (IRIS), U.S. Environmental Protection Agency, Washington, DC, 2011.
- [5] H.H. Russell, J.E. Matthews, G.W. Sewell, TCE removal from contaminated soil and ground water. Ground water issue, Environ. Protect. Agency (1992) 12.
- [6] W.J. Blanford, E.J. Kringel, G.R. Johnson, R.B. Cain, C. Enfield, M.L. Brusseau, 725 (1999) 167–181.
- [7] G.V. Lowry, M. Reinhard, Environ. Sci. Technol. 35 (2001) 696–702.
- [8] S. Ordóñez, H. Sastre, F.V. Díez, Appl. Catal. B: Environ. 25 (2000) 49–58.
- [9] D.I. Kim, D.T. Allen, Ind. Eng. Chem. Res. 36 (1997) 3019–3026.
- [10] M.G. Davie, H. Cheng, G.D. Hopkins, C.A. Lebron, M. Reinhard, Environ. Sci. Technol. 42 (2008) 8908–8915.
- [11] M. Zhang, D.B. Bacik, C.B. Roberts, D. Zhao, Water Res. 47 (2013) 3706–3715.
- [12] M. Cobo, J. Becerra, M. Castelblanco, B. Cifuentes, J.A. Conesa, J. Environ. Manage. 158 (2015) 1–10.
- [13] B. Schrick, J.L. Blough, A.D. Jones, T.E. Mallouk, Chem. Mater. 14 (2002) 5140–5147.
- [14] C.J. Lin, Y.H. Liou, S.L. Lo, Chemosphere 74 (2009) 314–319.
- [15] B.T. Meshesha, N. Barrabés, K. Föttinger, R.J. Chimentão, J. Llorca, F. Medina, G. Rupprechter, J.E. Sueiras, Appl. Catal. B: Environ. 117–118 (2012) 236–245.
- [16] B.T. Meshesha, N. Barrabés, J. Llorca, A. Dafinov, F. Medina, K. Föttinger, Appl. Catal. A: Gen. 453 (2013) 130–141.
- [17] N. Barrabés, D. Cornado, K. Foetttinger, A. Dafinov, J. Llorca, F. Medina, G. Rupprechter, J. Catal. 263 (2009) 239–246.
- [18] M.O. Nutt, K.N. Heck, P. Alvarez, M.S. Wong, Appl. Catal. B: Environ. 69 (2006) 115–125.
- [19] M.O. Nutt, J.B. Hughes, M.S. Wong, Environ. Sci. Technol. 39 (2005) 1346–1353.
- [20] L. Ren, X. Pan, Catal. Commun. 12 (2011) 1366–1369.
- [21] H. Takashima, M. Karches, Y. Kanno, Appl. Surf. Sci. 254 (2008) 2023–2030.
- [22] M. Cobo, C.A. González, E.G. Sánchez, C. Montes, Catal. Today 172 (2011) 78–83.
- [23] E. Díaz, A. McCall, L. Faba, H. Sastre, S. Ordóñez, Environ. Prog. Sustain. Energy 32 (2013) 1217–1222.
- [24] F.-D. Kopinke, K. Mackenzie, R. Koehler, A. Georgi, Appl. Catal. A: Gen. 271 (2004) 119–128.
- [25] S. Ordóñez, B.P. Vivas, F.V. Diez, Appl. Catal. B Environ. 95 (2010) 288–296.
- [26] W. Nishijima, Y. Ochi, T.-Y. Tsai, Y. Nakano, M. Okada, Appl. Catal. B: Environ. 51 (2004) 135–140.
- [27] S. Ordóñez, H. Sastre, F.V. Díez, Thermochim. Acta 379 (2001) 25–34.
- [28] S. Ordóñez, F.V. Díez, H. Sastre, Appl. Catal. B: Environ. 31 (2001) 113–122.
- [29] N. Munakata, M. Reinhard, Appl. Catal. B: Environ. 75 (2007) 1–10.
- [30] G.V. Lowry, M. Reinhard, Environ. Sci. Technol. 34 (2000) 3217–3223.
- [31] F.-D. Kopinke, D. Angeles-Wedler, D. Fritsch, K. Mackenzie, Appl. Catal. B: Environ. 96 (2010) 323–328.
- [32] R. Navon, S. Eldad, K. Mackenzie, F.-D. Kopinke, Appl. Catal. B: Environ. 119–120 (2012) 241–247.
- [33] C.M. Burkett, P.L. Edmiston, J. Non-Cryst. Solids 351 (2005) 3174–3178.
- [34] C.M. Burkett, L.A. Underwood, R.S. Volzer, J.A. Baughman, P.L. Edmiston, Chem. Mater. 20 (2008) 1312–1321.
- [35] P.L. Edmiston, L.A. Underwood, Sep. Purif. Technol. 66 (2009) 532–540.
- [36] P.L. Edmiston, in: U.S. Patent (Ed.), Swellable Sol-Gels, Methods of Making, and Use Thereof, c08g77/60 ed., Abs Materials, Inc., United States, 2012.
- [37] P.L. Edmiston, in: U.S. Patent (Ed.), Swellable Materials and Methods of Use, c08g77/60 ed., Abs Materials, Inc., United States, 2013.

- [38] F.A. Miller, J. Raman Spectrosc. 19 (1988) 219–221.
- [39] D.A. Oriero, A.T. Weakley, D.E. Aston, Sci. Technol. Adv. Mater. 13 (2012), 025008 (10pp).
- [40] N. Colthup, Introduction to Infrared and Raman Spectroscopy, Elsevier, 2012.
- [41] A. Martinelli, Int. J. Mol. Sci. 15 (2014) 6488–6503.
- [42] A. Bertoluzza, C. Fagnano, M.A. Morelli, V. Gottardi, M. Guglielmi, J. Non-Cryst. Solids 48 (1982) 117–128.
- [43] R. Lorenzi, S. Brovelli, F. Meinardi, A. Lauria, N. Chiodini, A. Paleari, J. Non-Cryst. Solids 357 (2011) 1838–1841.
- [44] D.J. Little, M. Ams, P. Dekker, G.D. Marshall, J.M. Dawes, M.J. Withford, Opt. Express 16 (2008) 20029–20037.
- [45] G. Socrates, Infrared and Raman Characteristic Group Frequencies: Tables and Charts, John Wiley & Sons, 2004.
- [46] B.A. Morrow, J. Phys. Chem. 81 (1977) 2663–2666.
- [47] P.J. Launer, Silicone compounds register and review 100 (1987).
- [48] F. Galeener, G. Lucovsky, Phys. Rev. Lett. 37 (1976) 1474.
- [49] M. Payne, J. Inkson, J. Non-Cryst. Solids 68 (1984) 351–360.
- [50] S. De Leeuw, M.F. Thorpe, Phys. Rev. Lett. 55 (1985) 2879.
- [51] R.M. Almeida, C.G. Pantano, J. Appl. Phys. 68 (1990) 4225–4232.
- [52] D. Lin-Vien, N.B. Colthup, W.G. Fateley, J.G. Grasselli, The Handbook of Infrared and Raman Characteristic Frequencies of Organic Molecule, Elsevier, 1991.
- [53] J. Fan, J.T. Yates, J. Am. Chem. Soc. 118 (1996) 4686–4692.
- [54] E. Mendelovici, R. Villalba, A. Sagarzazu, O. Carias, Clay Miner. 30 (1995) 307–313.
- [55] B. de Rivas, R. López-Fonseca, J.R. González-Velasco, J.I. Gutiérrez-Ortiz, Catal. Commun. 9 (2008) 2018–2021.
- [56] P.S. Chintawar, H.L. Greene, J. Catal. 165 (1997) 12–21.
- [57] G. Yuan, M.A. Keane, Catal. Today 88 (2003) 27–36.
- [58] H. Watanabe, T. Hosoi, Physics and Technology of Silicon Carbide Devices, 2013, pp. 235–250.
- [59] M. Kim, J. Kim, Phys. Chem. Chem. Phys. 16 (2014) 11323–11336.
- [60] A. Yamashita, Y. Sato, T. Tsukamoto, Y. Suda, Appl. Phy. Exp. 7 (2014) 074203.
- [61] R. Wojcieszak, M. Ghazzal, E.M. Gaigneaux, P. Ruiz, Catal. Sci. Technol. 4 (2014) 738–745.
- [62] D. Wang, S. Lu, P.J. Kulesza, C.M. Li, R. De Marco, S.P. Jiang, Phys. Chem. Chem. Phys. 13 (2011) 4400–4410.
- [63] X. Liu, G. Xu, Y. Chen, T. Lu, Y. Tang, W. Xing, Sci. Rep. 5 (2015).